Infrared Absorption Spectrum of the Simplest Criegee Intermediate CH_2OO

Yu-Te Su *et al.*

Science **340**, 174 (2013);
DOI: 10.1126/science.1234369

Infrared Absorption Spectrum of the Simplest Criegee Intermediate CH_2OO

Yu-Te Su,[1] Yu-Hsuan Huang,[1] Henryk A. Witek,[1]* Yuan-Pern Lee[1,2]*

The Criegee intermediates are carbonyl oxides postulated to play key roles in the reactions of ozone with unsaturated hydrocarbons; these reactions constitute an important mechanism for the removal of unsaturated hydrocarbons and for the production of OH in the atmosphere. Here, we report the transient infrared (IR) absorption spectrum of the simplest Criegee intermediate CH_2OO, produced from $CH_2I + O_2$ in a flow reactor, using a step-scan Fourier-transform spectrometer. The five observed bands provide definitive identification of this intermediate. The observed vibrational frequencies are more consistent with a zwitterion rather than a diradical structure of CH_2OO. The direct IR detection of CH_2OO should prove useful for kinetic and mechanistic investigations of the Criegee mechanism.

The gaseous reactions of ozone (O_3) with unsaturated hydrocarbons have been extensively investigated, given their roles in atmospheric depletion of these molecules and associated build-up of OH free-radical and particulate material in the troposphere (*1*–*3*). In summer, the dominant OH-production channel in the atmosphere includes photolysis of ozone to produce $O(^1D)$, which subsequently reacts with H_2O to produce OH. During the winter season, the efficiency of ozone photolysis drops by 50% or more, and the atmospheric production of OH via ozonolysis of alkenes was proposed to account for the difference in the photolytic production of OH between summer and winter (*4*).

Decades of research suggest the initiation of the ozonolysis reactions involves the cycloaddition of ozone to the C=C double bond to form a cyclic trioxolane intermediate (ozonide) with a C–C single bond. The large exothermicity of this reaction leads to a rapid cleavage of this C–C bond and one O–O bond of the ozonide to form a carbonyl molecule and a carbonyl oxide that is commonly referred to as the Criegee intermediate, which was first postulated by Criegee in 1949 (*5*). The simplest ozone-alkene reaction involves ethene (C_2H_4); the products from fragmentation of ethene ozonide ($C_2H_4O_3$) are formaldehyde (H_2CO) and formaldehyde oxide (or peroxymethylene, CH_2OO), which is hence the simplest Criegee intermediate. The structure and reactions of gaseous Criegee intermediates have been extensively investigated and debated (*6*–*9*). Four isomers of CH_2O_2 include formaldehyde oxide, dioxirane, methylenebis(oxy), and formic acid (HCOOH), as shown in Fig. 1. The large exothermicity of the reaction of $O_3 + C_2H_4$ might lead to isomerization among these isomers and the decomposition of these species to produce H, OH, CH_3, CO, CO_2, and other products (*1*–*3*).

The highly reactive Criegee intermediates have until recently eluded detection in the gaseous phase. Taatjes and co-workers produced CH_2OO from the reactions of $CH_3SOCH_2 + O_2$ (*10*) and $CH_2I + O_2$ (*11*) in a flow cell and detected its cation with vacuum ultraviolet photoionization. They confirmed that the Criegee intermediate, rather than other isomers, was observed because the observed photoionization threshold near 10 eV conforms to theoretical predictions of 9.98 eV (*12*), which is much smaller than the values of 10.82 eV predicted for dioxirane (*12*) and 11.3 eV determined for formic acid (*13*). Beames *et al*. used the $CH_2I + O_2$ reaction to prepare CH_2OO in a supersonic jet and reported that a broad ultraviolet (UV) spectrum of CH_2OO peaked near 335 nm; the spectrum was obtained through UV-induced depletion of the ion signal of CH_2OO produced upon photoionization (*14*). The infrared (IR) absorption spectrum of gaseous CH_2OO would supply more detailed structural information as well as an alternative means for performing kinetic measurements.

Theoretical investigations of the structure and reactivity of CH_2OO have been extensive (*12*, *15*–*18*), but predictions of the enthalpy of formation, electronic structure, and vibrational wave numbers vary considerably. The reported enthalpy of formation of CH_2OO at 298 K, ΔH_f^0, varies from 26 to 48 kcal mol^{-1} but settles toward the smaller value when more sophisticated methods are used. Earlier theoretical calculations indicated CH_2OO to have a planar, singlet biradical structure, with nearly equally long O–O and C–O bonds of about 1.34 Å (*19*), whereas coupled-cluster theory CCSD(T) and multiconfigurational complete active space self-consistent field (CASSCF) calculations predicted that CH_2OO is better described as a zwitterion with a shorter C–O bond (~1.28 Å) and a longer O–O bond (~1.35 Å) (Fig. 1A) (*12*, *16*, *17*). The vibrational frequencies predicted for CH_2OO also vary considerably. For example, predictions of the wave number of the O–O stretching mode ranged from 849 to 1077 cm^{-1}, and of the C–O stretching mode from 1269 to 1407 cm^{-1}.

Because CH_2OO is unstable, its detection with a conventional Fourier-transform IR (FTIR) spectrometer is difficult. We have demonstrated that coupling a step-scan FTIR spectrometer with a multipass absorption cell enables the recording of temporally resolved IR absorption spectra of gaseous reaction intermediates such as ClCO (*20*) and CH_3OO (*21*); distinct absorption bands of various isomers of CH_3SO_2 (*22*), CH_3SOO (*23*), and CH_3OSO (*24*) were recorded to provide definitive structural identification. Here, we report a further application of this technique to characterize the IR absorption spectra of gaseous CH_2OO species.

A step-scan FTIR [Vertex 80v (Bruker Optik, Ettlingen, Germany)] spectrometer coupled with a multireflection White cell was used to record the IR spectra of transient species. The laser beam, of wavelength 248 nm, passed through the White cell and was reflected six times with two external mirrors so as to photodissociate a flowing mixture of CH_2I_2 in N_2/O_2 and thereby produced CH_2I that subsequently reacted with O_2 to form CH_2OO. The derivation of conventional time-resolved difference absorption spectra from the temporal profiles recorded at each scan step has been established (*20*, *25*).

The partial IR absorption spectrum (800 to 1500 cm^{-1}) of the flowing mixture of $CH_2I_2/N_2/O_2$ (1/20/760, 94 torr) at 340 K (Fig. 2A) exhibits absorption lines of CH_2I_2 near 1229, 1188, and 1113 cm^{-1}. Upon irradiation with light at 248 nm, the absorption of CH_2I_2 decreased owing to photolysis, whereas new bands near 1435, 1286, 908, and 848 cm^{-1} appeared, as shown in the difference spectrum recorded at 0- to 12.5-μs delays (Fig. 2B); a band with a weak Q-branch near 1241 cm^{-1} (indicated by an arrow) might belong to the same group but is interfered with by absorption of parent or other products. The intensities of these new lines decreased rapidly with time and diminished after ~100 μs; a spectrum recorded 50 to 62.5 μs after photo-irradiation is shown in Fig. 2C. The decay of CH_2OO resulted in increased absorption of H_2CO.

Because photolysis of CH_2I_2 produces mainly the CH_2I radical (*26*) and because this radical reacts readily with excess O_2 in the system (*27*, *28*), the possible carriers of the observed new bands include CH_2IOO and isomers of CH_2O_2. Most pre-

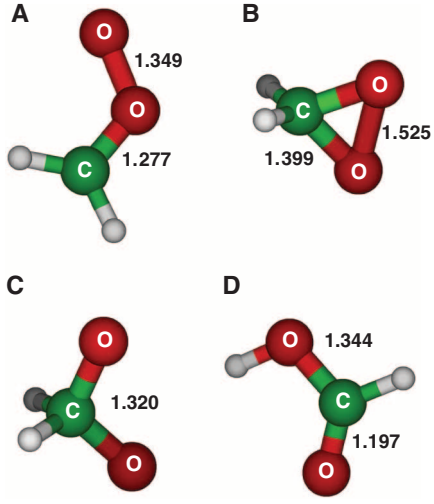

Fig. 1. Geometries of possible isomers of CH_2O_2. (**A**) Formaldehyde oxide CH_2OO, (**B**) dioxirane, (**C**) methylenebis(oxy), and (**D**) formic acid predicted with the NEVPT2/aVTZ method [(A) to (C)] and the B3LYP/aVTZ method (D). The O–O and C–O bond distances are given in angstroms.

[1]Department of Applied Chemistry and Institute of Molecular Science, National Chiao Tung University, 1001, Ta-Hsueh Road, Hsinchu 30010, Taiwan. [2]Institute of Atomic and Molecular Sciences, Academia Sinica, Taipei 10617, Taiwan.

*Corresponding author. E-mail: yplee@mail.nctu.edu.tw (Y.-P.L.); hwitek@mail.nctu.edu.tw (H.W.)

vious experimental attempts to generate and detect CH_2OO used either the reaction of $CH_2 + O_2$ or $C_2H_4 + O_3$, but the large exothermicity of these reactions makes the stabilization of CH_2OO difficult. In contrast, in the reaction of $CH_2I + O_2 \rightarrow CH_2OO + I$ chosen here, the stabilization of CH_2OO is possible because of the small exothermicity of ~13 kJ mol^{-1}.

The observed vibrational wave numbers and relative intensities are compared with theoretical predictions for CH_2OO in Table 1. Previous investigations (*12*, *18*) reported only harmonic vibrational frequencies, so we performed new calculations in order to derive the anharmonic frequencies. The potentially zwitterionic character of the CH_2OO molecule requires appropriate multireference treatment. The harmonic and anharmonic vibrational frequencies have been computed by using a quadratic force field obtained with the *n*-electron valence state perturbation theory (NEVPT2) method (*29*) implemented in the Molpro quantum chemistry package (*30*) by using the CASSCF(8,8) reference wave function. No symmetry has been used in these calculations so as to avoid numerical problems. The anharmonic frequencies (*31*) have only approximate character because the effects of three- and four-mode couplings have been neglected owing to high computational complexity. Nevertheless, the computed NEVPT2/aVDZ anharmonic frequencies correspond well to the observed experimental bands.

The IR spectra of CH_2OO, dioxirane, methylenebis(oxy), and cis-CH_2IOO simulated according to the geometries and anharmonic vibrational frequencies that were predicted with quantum-chemical calculations are shown in Fig. 2, D to G, respectively. A compilation of anharmonic vibrational levels and IR intensities for the isomers of CH_2OO and other possible intermediate structures used in the simulations is given in tables S1 and S2. The rotational constants used in the simulation are compiled in table S3. For CH_2IOO and CH_2OO, the characteristic OO-stretching modes have wave numbers near 900 cm^{-1}. For dioxirane, two intense features near 1238 and 911 cm^{-1} are characteristic of symmetric and antisymmetric CO-stretching modes (*17*). For methylenebis(oxy), only an anharmonic NEVPT2 (2,2) stick spectrum is shown because the B3LYP (Becke, three-parameter, Lee-Yang-Parr) rotational constants for each fundamental mode could not be assessed (supplementary text). A comparison of the observed new spectral features with these simulated spectra indicates that the best agreement in terms of relative intensities and positions is obtained for the predicted spectrum of CH_2OO. The Criegee intermediate is predicted to have intense lines at 1458 (52), 1302 (100), 1220 (33), 892 (100), and 853 (31) cm^{-1}; the relative IR intensities are listed in parentheses. The observed features are at 1435 (33), 1286 (42), 1241 (39), 908 (100), and 848 (24) cm^{-1}, with typical deviations of 5 to 23 cm^{-1} from predicted anharmonic vibrational wave numbers. The predicted spectra of other candidate species disagree with the observed spectrum. For example, although dioxirane is predicted to have two intense lines near 1238 and 911 cm^{-1}, near the observed features at 1286 and 848 cm^{-1} the relative intensities and the rotational contours do not match. The widths of the rotational contours of bands of CH_2IOO are predicted to be much smaller than the observed widths because the massive I atom induces small rotational parameters; the possibility that the observed new features are due to CH_2IOO is positively eliminated. In contrast, the predicted rotational contours of each vibrational band of CH_2OO agree well with observations, except for a weak Q-branch near 1241 cm^{-1} that might experience interference from absorption of the precursor or other product. A comparison of observed and simulated rotational contours for the ν_6 and ν_8 modes is shown in Fig. 3; those for the ν_3 and ν_4/ν_5 modes are shown in figs. S1 and S2, respectively. Most bands of CH_2OO have a mixed *a*/*b*-type contour with P-, Q-, and R-branches, whereas the out-of-plane CH_2-wagging (ν_8) mode near 848 cm^{-1}

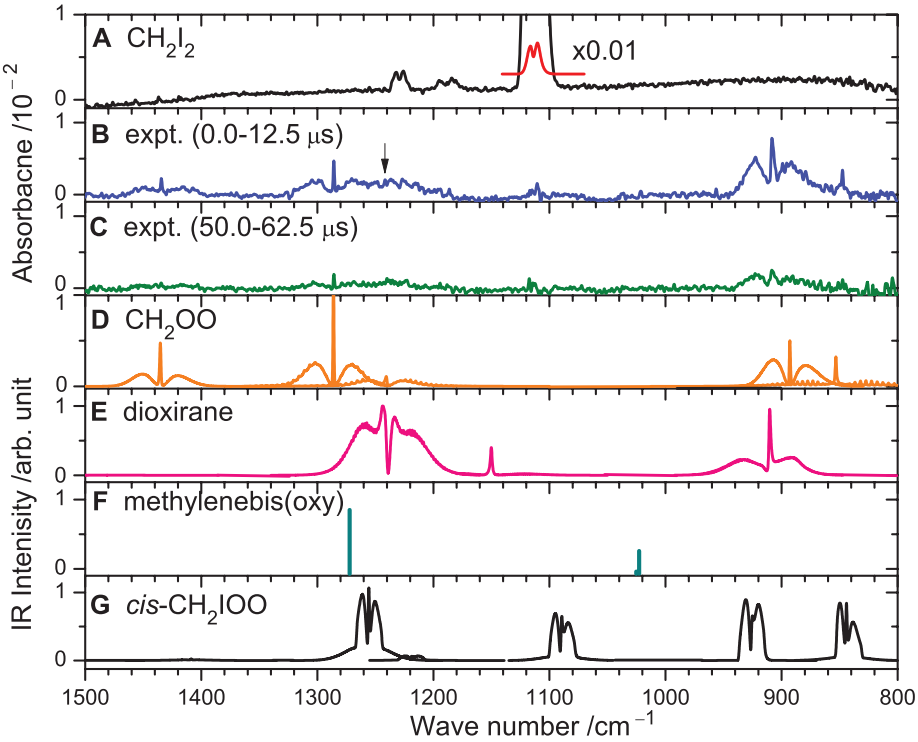

Fig. 2. Comparison of observed spectra with simulated spectra of possible species. (**A**) IR absorption spectrum of a flowing mixture of $CH_2I_2/N_2/O_2$(1/20/760, 94 torr) before photolysis. (**B**) Difference spectra recorded 0 to 12.5 μs and (**C**) 50 to 62.5 μs after irradiation of the sample at 248 nm; the spectrum at 300 to 312.5 μs was subtracted for background correction. IR spectra of (**D**) CH_2OO, (**E**) dioxirane, (**F**) methylenebis(oxy), and (**G**) cis-CH_2IOO were simulated by using the predicted rotational constants, vibrational frequencies, and IR intensities listed in tables S1 and S3.

Table 1. Comparison of experimentally observed wave numbers (per centimeter) and intensities with the vibrational wave numbers (per centimeter) and IR intensities of CH_2OO predicted with various methods. Sym., symmetry.

Mode	Sym.	Experiment	NEVPT2/aVDZ		CAS(14,12)	CCSD(T)	Description†
			Harmonic	Anharmonic	/VDZ*	/aVTZ*	
ν_1	A′		3370	3149 (5)‡	3215	3290	*a*-CH str.
ν_2	A′		3197	3030 (1)	3065	3137	*s*-CH str.
ν_3	A′	1435 (33)§	1500	1458 (52)	1465	1483	CH_2 scissor/CO str.
ν_4	A′	1286 (42)	1338	1302 (100)	1269	1306	CO str./CH_2 scissor
ν_5	A′	1241 (39)	1235	1220 (33)	1233	1231	CH_2 rock
ν_6	A′	908 (100)	916	892 (100)	849	935	OO str.
ν_7	A′		536	530 (1)	537	529	COO deform
ν_8	A″	848 (24)	856	853 (31)	793	862	CH_2 wag
ν_9	A″		620	606 (2)	618	632	CH_2 twist
Reference		This work	This work	This work	(*18*)	(*12*)	

*Harmonic wave numbers. †Approximate mode description. *a*, asymmetric; *s*, symmetric; str., stretch. ‡Relative IR intensities are normalized to the most intense line (ν_4) with intensity 124 km mol^{-1}. §Integrated IR intensities relative to ν_6 are listed in parentheses.

has a characteristic *c*-type structure with a prominent Q-branch because the dipole moment oscillates mainly along the *c* axis (perpendicular to the molecular plane) upon vibrational excitation. This unique *c*-type feature of a planar molecule near 848 cm^{-1} further supports the assignment of the observed features to CH_2OO.

The observed wave number of the OO-stretching mode of CH_2OO near 908 cm^{-1} is much smaller than that of the corresponding modes of CH_3OO at 1117 cm^{-1} (*21*), $CH_3C(O)OO$ (*32*) at 1102 cm^{-1}, and $C_6H_5C(O)OO$ at 1108 cm^{-1} (*33*) determined with a similar technique. The observed wave number of the CO-stretching mode near 1286 cm^{-1} is much larger than that of the corresponding mode of CH_3OO at 902 cm^{-1} (*34*) observed in a matrix, indicating some double-bond character. These trends strongly support a zwitterionic, rather than singlet biradical, structural description of CH_2OO because of a strengthened C–O bond and a weakened O–O bond.

The ~50-μs lifetime of CH_2OO observed in our experiment is much shorter than that (~2 ms) reported by Welz *et al.* (*11*), who used $[CH_2I]_0 \cong 9\times10^{11}$ molecules cm^{-3} in their experiments. Because the sensitivity of IR absorption is not as good as that of mass detection, a higher concentration of $[CH_2I]_0 \cong 4\times10^{13}$ molecules cm^{-3} is needed in our experiments in order to record a satisfactory spectrum of CH_2OO. In some preliminary low-resolution experiments, we varied $[CH_2I]_0$ from 1.0×10^{13} to 2.8×10^{14} molecules cm^{-3} and found that the lifetime of CH_2OO decreased from ~150 to 15 μs, indicating that the bimolecular reaction—either $CH_2OO + I$ or $CH_2OO + CH_2OO$—might be responsible for this rapid decay. More detailed kinetic measurements are in progress.

With our detection method, we can probe CH_2OO directly in a reaction. The advantage is demonstrated in the investigation of the yield of CH_2OO from the reaction $CH_2I + O_2$. Solar photolysis of CH_2I_2, one major source of iodine in the marine boundary layer, generates CH_2I and I. The reaction of $CH_2I + O_2$ is important in the atmosphere partly because this reaction releases the second I atom to form IO, which can affect O_3, HO_x, and NO_x levels and also lead to the formation of particulates in the atmosphere (*35*). Huang *et al.* detected I atom as a product of the reaction of CH_2I with O_2 by probing the IR absorption of I atom at 7603.138 cm^{-1}. These authors reported that O_2 stabilizes CH_2IOO with remarkable efficiency (13 times that of N_2), hence decreasing the yield of I atoms (*28*). The yield of CH_2OO from $CH_2I + O_2$ was estimated to be 0.04 in air at 760 torr because CH_2IOO is expected to be readily stabilized. However, because these authors probed only I atoms, their measurements could not distinguish between the stabilization of CH_2IOO and other secondary reactions. With our new detection method, we can probe CH_2OO directly to provide direct measurements of the yield of CH_2OO. Contrary to their predictions, in our experiment with O_2 at 90 torr we observed no CH_2IOO, and the yield of CH_2OO was estimated to be at least 35% of CH_2I with the assumption that the predicted IR intensities of CH_2OO are correct. Whether this discrepancy is due to the difference in photolysis wavelengths [355 nm in experiments of Huang *et al.* (*28*) and 248 nm in this work]—in which the total available energy of $CH_2I + I$ (118 and 263 kJ mol^{-1}, respectively) might affect the efficiency of stabilization of CH_2IOO and CH_2OO produced from $CH_2I + O_2$—requires further investigation.

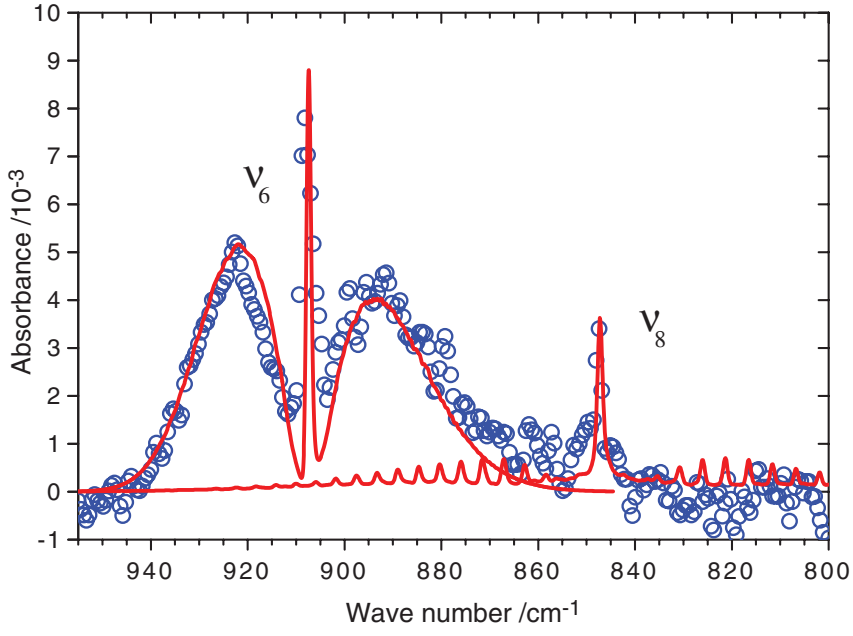

Fig. 3. Comparison of observed and simulated spectra of CH_2OO in the region of 800 to 955 cm^{-1} at resolution 1.0 cm^{-1}. Simulated absorption bands for the ν_6 (ν_0 = 908 cm^{-1} and *a*-/*b*-type = 8.2/1) and ν_8 (ν_0 = 848 cm^{-1} and *c*-type) modes are shown with red lines, and the observed spectrum is shown with open circles. Spectral width = 1 cm^{-1}, J_{max} = 150, and T = 340 K.

References and Notes

1. D. Johnson, G. Marston, *Chem. Soc. Rev.* **37**, 699 (2008).
2. J. G. Calvert *et al.*, *The Mechanisms of Atmospheric Oxidation of the Alkenes* (Oxford University Press, Oxford, UK, 2000), pp. 172–335.
3. O. Horie, G. Moortgat, *Acc. Chem. Res.* **31**, 387 (1998).
4. R. M. Harrison *et al.*, *Sci. Total Environ.* **360**, 5 (2006).
5. R. Criegee, G. Wenner, *Chem. Ber.* **9**, 564 (1949).
6. W. Sander, *Angew. Chem. Int. Ed. Engl.* **29**, 344 (1990).
7. W. H. Bunnelle, *Chem. Rev.* **91**, 335 (1991).
8. S. Hatakeyama, H. Akimoto, *Res. Chem. Intermed.* **20**, 503 (1994).
9. G. Marston, *Science* **335**, 178 (2012).
10. C. A. Taatjes *et al.*, *J. Am. Chem. Soc.* **130**, 11883 (2008).
11. O. Welz *et al.*, *Science* **335**, 204 (2012).
12. M. T. Nguyen, T. L. Ngyuen, V. T. Ngan, H. M. T. Ngyuen, *Chem. Phys. Lett.* **448**, 183 (2007) and references therein.
13. T. A. Cool, J. Wang, K. Nakajima, C. A. Taatjes, A. McIlroy, *Int. J. Mass Spectrom.* **247**, 18 (2005).
14. J. M. Beames, F. Liu, L. Lu, M. I. Lester, *J. Am. Chem. Soc.* **134**, 20045 (2012).
15. J. M. Anglada, J. González, M. Torrent-Sucarrat, *Phys. Chem. Chem. Phys.* **13**, 13034 (2011).
16. L. Vereecken, J. S. Francisco, *Chem. Soc. Rev.* **41**, 6259 (2012).
17. D. Cremer, J. Gauss, E. Kraka, J. F. Stanton, R. J. Bartlett, *Chem. Phys. Lett.* **209**, 547 (1993).
18. D.-C. Fang, X.-Y. Fu, *J. Phys. Chem. A* **106**, 2988 (2002) and references therein.
19. L. B. Harding, W. A. Goddard, *J. Am. Chem. Soc.* **100**, 7180 (1978).
20. S.-H. Chen, L.-K. Chu, Y.-J. Chen, I.-C. Chen, Y.-P. Lee, *Chem. Phys. Lett.* **333**, 365 (2001).
21. D.-R. Huang, L.-K. Chu, Y.-P. Lee, *J. Chem. Phys.* **127**, 234318 (2007).
22. L.-K. Chu, Y.-P. Lee, *J. Chem. Phys.* **124**, 244301 (2006).
23. L.-K. Chu, Y.-P. Lee, *J. Chem. Phys.* **133**, 184303 (2010).
24. J.-D. Chen, Y.-P. Lee, *J. Chem. Phys.* **134**, 094304 (2011).
25. Materials and methods are available as supplementary materials on *Science* Online.
26. S. L. Baughcum, S. R. Leone, *J. Chem. Phys.* **72**, 6531 (1980).
27. T. J. Gravestock, M. A. Blitz, W. J. Bloss, D. E. Heard, *ChemPhysChem* **11**, 3928 (2010).
28. H. Huang, A. J. Eskola, C. A. Taatjes, *J. Phys. Chem. Lett.* **3**, 3399 (2012).
29. C. Angeli, R. Cimiraglia, S. Evangelisti, T. Leininger, J. P. Malrieu, *J. Chem. Phys.* **114**, 10252 (2001).
30. H.-J. Werner, P. J. Knowles, G. Knizia, F. R. Manby, M. Schütz, *WIREs Comput. Mol. Sci.* **2**, 242 (2012).
31. M. Neff, G. Rauhut, *J. Chem. Phys.* **131**, 124129 (2009).
32. S.-Y. Chen, Y.-P. Lee, *J. Chem. Phys.* **132**, 114303 (2010).
33. B. Golec, J.-D. Chen, Y.-P. Lee, *J. Chem. Phys.* **135**, 224302 (2011).
34. S. Nandi *et al.*, *J. Phys. Chem. A* **106**, 7547 (2002).
35. G. McFiggans *et al.*, *Atmos. Chem. Phys.* **4**, 701 (2004).

Acknowledgments: Calculation details and a compilation of anharmonic vibrational levels and IR intensities for possible intermediate structures with additional simulation plots are presented in the supplementary materials. National Science Council of Taiwan (grants NSC102-2745-M009-001-ASP and NSC99-2113-M-009-011-MY3) and the Ministry of Education, Taiwan ("Aim for the Top University Plan" of National Chiao Tung University) supported this work. The National Center for High-Performance Computing provided computer time. We thank G. Rauhut for his assistance in the calculations of anharmonic vibrational frequencies.

Supplementary Materials

www.sciencemag.org/cgi/content/full/340/6129/174/DC1
Materials and Methods
Supplementary Text
Figs. S1 and S2
Tables S1 to S3
References (*36*–*44*)

20 December 2012; accepted 1 March 2013
10.1126/science.1234369